Widefield fluorescence localization microscopy for transcranial imaging of cortical perfusion with capillary resolution

Chen, Zhenyue ; Zhou, Quanyu ; Robin, Justine ; Razansky, Daniel

DOI: https://doi.org/10.1364/ol.396123

Widefield fluorescence localization microscopy (WFLM) for transcranial imaging of cortical perfusion with capillary resolution

ZHENYUE CHEN[1,2], QUANYU ZHOU[1,2], JUSTINE ROBIN[1,2], AND DANIEL RAZANSKY[1,2,*]

1 Faculty of Medicine and Institute of Pharmacology and Toxicology, University of Zurich, Switzerland
2 Institute for Biomedical Engineering and Faculty of Information Technology and Electrical Engineering, ETH Zurich, Switzerland
** Corresponding author: daniel.razansky@uzh.ch*

Received XX Month XXXX; revised XX Month, XXXX; accepted XX Month XXXX; posted XX Month XXXX (Doc. ID XXXXX); published XX Month XXX

Imaging of cerebral vasculature is impeded with the existing fluorescence microscopy methods due to intense light scattering in living tissues and the need for highly invasive craniotomy procedures to resolve structures on a capillary scale. We propose a widefield fluorescence localization microscopy (WFLM) technique for high-resolution transcranial imaging and quantitative assessment of cortical perfusion in mice. The method is based on tracking single fluorescent microparticles sparsely distributed in the blood stream using a simple CMOS camera and a continuous wave laser source. We demonstrate quantitative transcranial in vivo mapping of the blood flow velocity and direction at capillary level resolution (5μm) across the entire cortex. The new technique opens a new high resolution transcranial window into the brain function in health and disease. © 2020 Optical Society of America

http://dx.doi.org/

Cerebral micro-angiography is a crucial tool in understanding the vascular function that directs brain development, regulates homeostasis, and contributes to pathological processes [1]. It is also of paramount importance for diagnosis and treatment in various brain diseases such as stroke, neurodegenerative disorders, and brain cancer [2-4]. Ex vivo optical imaging methods (e.g. light-sheet microscopy, expansion microscopy) have been reported for studies into large-scale brain vascular networks with capillary resolution, yet those approaches involve tissue clearing making them unsuitable for in vivo application [5, 6]. On the other hand, whole-brain imaging modalities such as X-ray computed tomography (CT) and magnetic resonance imaging (MRI) have been applied to study the brain vasculature both preclinically and clinically [7, 8]. Despite relatively high resolution achieved for in vivo studies, the micro-CT and –MRI methods are associated with high complexity, cost and radiation dose (for micro-CT), lengthy acquisition times and poor molecular sensitivity. Optoacoustics has shown great scalability for angiographic imaging, from optical resolution microscopy at superficial depths to centimeter-scale penetration with acoustic resolution methods [9, 10]. Yet, high-resolution imaging of microvasculature at the whole cortex scale is associated with long scanning times, impeding visualization of fast biodynamics. Optical coherence tomography angiography (OCTA) has been reported to quantitatively assess transcranial blood perfusion in the mouse cortex using Doppler down to the capillary level [11]. The lateral resolution of OCTA is typically limited to 10 μm while it can only measure velocities along the axial direction, further failing to detect red blood cell velocities [12]. Laser speckle contrast imaging (LSCI) or laser speckle flowmetry were shown capable of visualizing the vasculature, blood flow and tissue perfusion by measuring the decrease in speckle contrast in a time-series of images [13, 14]. However, due to the equivocal relationship between decorrelation velocity and time, laser speckle contrast imaging is unable to achieve quantitative flow velocity results [15, 16]. Moreover, the spatial resolution for transcranial imaging is typically limited to the 40 μm range while the relatively low speckle contrast at high flow velocities makes those methods unsuitable for visualizing fast perfusion dynamics. To address the current limitations and unmet needs of murine cerebrovascular imaging, we propose a cost-effective, minimally invasive WFLM method capable of capillary resolution mapping of the cortical vascular network, blood velocity and flow direction.

The experimental setup is depicted in Fig. 1a. It comprises a sCMOS camera (pco.dimax S1, PCO AG, Germany), a 473 nm CW laser (FPYL-473-1000-LED, Frankfurt Laser Company, Germany) and a customized microscope. In order to capture the entire mouse cortex with high spatial resolution, a large FOV objective (CLS-SL, Thorlabs, USA) was employed. To match the sensor size of the sCMOS camera, a tube lens (TTL100-A, Thorlabs, USA) with 100 mm focal length was selected to obtain a magnification power of 1.43. For the epi-illumination, the 473 nm laser beam was first diverged and then deflected by a dichroic mirror (HCBS 495, AHF analysentechnik AG, Germany) into the objective to form uniform illumination upon the sample.

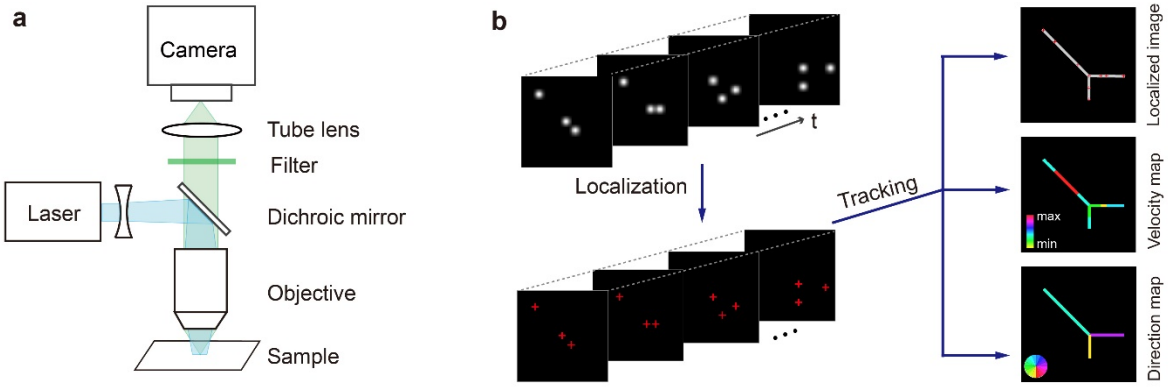

Figure 1. Experimental setup and principle of the widefield fluorescence localization microscopy (WFLM) and particle tracking. (a) Schematic drawing of the system setup. (b) Illustration of localization-based reconstruction and the process of estimating the velocity and direction of flow.

The principle of image processing is depicted in Fig. 1b. For localization microscopy and particle tracking, a stack of camera images was first acquired. The fluorescent emitters in each frame were localized by searching for local maxima with an adaptive threshold method while the centroid coordinates of blurring PSFs were recorded corresponding to different fluorescent beads locations. Subsequently, the trajectory of each recognizable emitter was tracked with simpletracker algorithm [17]. Two main parameters are involved to establish the linking of the same emitter in time-lapse frames: max-linking-distance (MLD) and max-gap-closing (MGC). The MLD parameter defines the acceptable displacement to search for the same beads between consecutive frames, which is dependent on the frame rate and potential flow velocity range. For instance, 50 μm distance is required for tracking velocities of up to 10 mm/s when operating at 200 Hz frame rate. MGC implies the maximum number of frames that could be skipped during the linking process - set to zero to avoid any potential false linking. An empirical threshold of linking length was used to only preserve effective linking. The localized image was subsequently rendered by superimposing all the particle trajectories while the brain-wide maps of flow velocity and direction were reconstructed by considering the relative displacement of each bead for the given fixed frame rate. Since the number of beads that flow across each pixel was random, the flow velocity and direction of each pixel were averaged accordingly. In addition, local velocity and flow direction in specific ROIs were acquired by calculating the correlations of two sub-images taken from adjacent frames with 8 x 8 pixel window size and 10 x 10 pixel step size. The flow velocity and direction were subsequently extracted from the correlation maps, which also verified the accuracy of the flow velocity and direction maps calculated by the simpletracker algorithm.

For a basic characterization of the proposed method, phantom experiments were performed by imaging fluorescent beads flowing through in a polythene tubing (0.28mm inner diameter, Smiths Medical International Ltd, UK). Orange-yellow fluorescent beads (FMOY-1.3, 460/594 nm, Cospheric, USA) with 1-5 μm diameter diluted in water were used for the injection. Flow velocity of the solution was controlled by a syringe pump and set to 3 mm/s. The frame rate of the camera was set to 40 Hz to record the entire injection process that lasted 5 s. The white light picture of the tubing network with a complex arrangement is shown in Fig. 2a along with the calculated velocity map of the fluorescent beads circulating in the tubing (Fig. 2b). As expected, the experimentally measured velocity was ~3 mm/s, in excellent agreement with the preset value by the syringe pump. WFLM is further able to accurately reconstruct the flow direction with the influx of beads originating from the top left corner and exiting at the bottom (Fig. 2c).

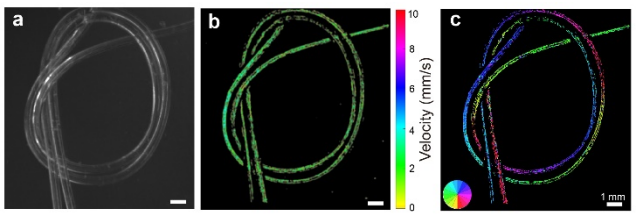

Fig. 2 Experimental characterization of the widefield fluorescence localization microscopy (WFLM) by imaging fluorescent beads flowing in a tubing phantom. (a) Photograph of the tubing. (b) The reconstructed velocity map. (c) The reconstructed flow direction map. Each color corresponds to one specific flow direction, as indicated by the color wheel. Scale bar: 1 mm.

In vivo validation was subsequently performed by imaging perfusion in the brain of a 2-month old athymic nude-Fox1nu mouse (Harlan Laboratories LTD, Switzerland). The same fluorescent beads (FMOY-1.3, 460/594 nm, Cospheric, USA) were diluted in PBS and administered intravenously through the tail vein. The mouse was anesthetized with isoflurane (3.0 % v/v for induction and 1.5 % v/v during experiments) in 20% O_2 and 80% air at a flow rate of ~1 l/min). During the experiment, the skull of the mouse was kept intact while the scalp was removed to reduce light scattering. To minimize bleeding, hemostatic sponges (Gelfoam®, Pfizer Pharmaceutical) were used together with a topical application of adrenaline. After the experiment, the animal was euthanized while still being under anesthesia. All experiments were performed in accordance with the Swiss Federal Act on Animal Protection and were approved by the Cantonal Veterinary Office Zurich.

The conventional widefield image of the mouse brain following injection of the Alexa Fluor 488 fluorescent dye is shown in Fig. 3a. As expected, due to the strong light scattering by the skull and the brain, the image was blurred out. In contrast, the localization-based image exhibits superior contrast and attains high spatial resolution on the capillary level across the entire mouse cortex (Fig. 3b). Fig. 3c depicts the color-coded blood flow velocity map. Since arterial vessels tend to have higher flow velocities as compared to the neighboring venous circulation, they are clearly discernable on the flow velocity map. Furthermore, when observing the reconstructed flow direction maps (Fig. 3d), the contradicting colors in the two hemispheres are indicative of the opposite flow directions. A detailed flow direction information is shown in Fig. 3e where the directivity is indicated by the arrows and the flow velocity is represented by the corresponding colors. Exemplary profiles of the temporal flow velocity variations in three vessels are plotted in Fig. 3f, further showcasing the type of quantitative functional information that can be extracted with our method when studying brain hemodynamics.

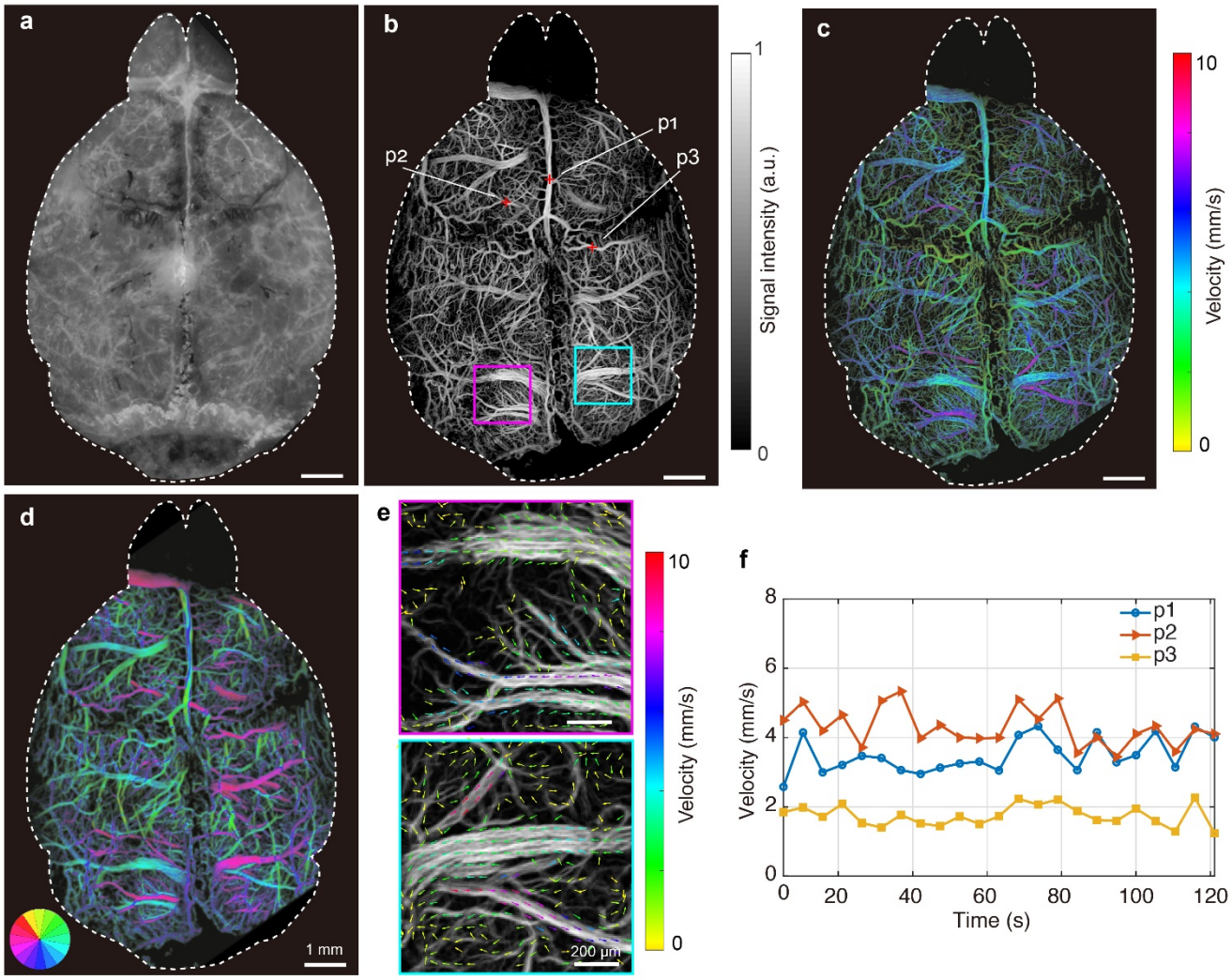

Fig. 3 Experimental results of imaging the mouse brain perfusion with the proposed WFLM technique. (a) Conventional widefield (planar) fluorescence image of the mouse brain perfused with Alexa Fluor 488 dye. (b) Mouse brain image reconstructed with WFLM. (c) Brain-wide velocity mapping with color-encoded flow velocity. (d) Brain-wide mapping of the flow directivity. (e) Combined velocity and flow direction map indicated with colors and arrows, respectively, in the two ROIs indicated in (b). (f) Temporal profiles of velocity variations in three representative vessels indicated in panel (b). Scale bar: (a)-(d) 1mm, (e) 200 μm.

The newly developed WFLM approach has distinct advantages over the conventional optical neuroimaging methods pertaining resolution, contrast and ease of operation. Although LSCI has been widely used for vascular imaging and tissue perfusion owing to its simplicity, it is unable to deliver quantitative readings of the flow velocity further providing inferior spatial resolution as compared to our proposed localization-based technique. Besides laser speckle contrast techniques, laser Doppler perfusion imaging has also been used to image the perfusion based on optical Doppler shifts calculated from the temporal intensity fluctuations caused by the dynamic speckle pattern. The lengthy scanning times associated with this method make it challenging to acquire images from large areas. The high-speed laser Doppler imaging system utilizing CMOS camera can achieve high-resolution flow images

(256x256 pixels) every 2 to 10 seconds, yet requiring a state-of-the-art high-speed camera with a frame-rate of 25 kHz [18]. We recently developed a high-speed large-field fluorescence imaging method based on multifocal structured illumination and acousto-optic deflectors for rapid beam steering and showcased its application to imaging of brain perfusion dynamics [19]. However, the spatial resolution achieved was inferior to the present work while further involving a highly sophisticated configuration featuring KHz frame rate camera, high repetition rate pulsed laser system and a complex beam splitting and deflection circuitry.

In this work, the hardware of the WFLM system requires an inexpensive camera running at hundred hertz and a CW laser for epi-illumination. To render a high-resolution structural image, the camera frame rate can be reduced to conventional video-rate since only the centroid of each tracking particle is used. However, to accurately map the blood flow velocity, the optimal camera frame rate is dependent on the particle velocity and magnification power of the imaging system. The maximum tracking speed, which is set to 10 mm/s, is directly restricted by the pre-defined max-linking-distance in the simpletracker algorithm. This parameter is selected according to the distribution density of beads in a single frame, which could be considered as sparse in the common case. The reconstruction algorithm performs adequately when the distance between difference beads is much greater than the max-linking-distance. Otherwise, the chances of false linking increase accordingly, thus impairing accuracy of the generated localized image and the corresponding flow velocity and direction maps. Note that we attempted using different tracking parameters in our image processing and reconstruction algorithms. In general, accuracy of the localization and flow mapping improved with the increased acquisition time when the same vessels are re-perfused multiple times. Yet, motion stabilization and retrospective gating acquisition may be required for imaging moving organs such as the beating murine heart [20, 21]. Potential strategies for maintaining accuracy while increasing the maximum tracking speed consist in reducing the concentration of the injected beads or using beads with different colors, which comes at the cost of losing temporal resolution or increased complexity of employing a multichannel imaging system. Alternatively, more expensive camera can be used with higher frame rates. However, reducing the exposure time would inevitably result in diminished SNR, thus undermining effectiveness of the beads' localization procedure. Other WFLM shortcomings include lack of depth resolving capacity and limited penetration depth. Future work may thus include development of 3D imaging abilities by exploiting astigmatism of a cylindrical lens or PSF-engineered phase masks [22, 23] to encode the depth information.

The proposed WFLM technique is also suitable for visualizing effects related to blood-brain-barrier (BBB) penetration, especially by means of fluorescent contrast agents in the superficial region of brain cortex. Indeed, the altered cerebrovascular integrity is closely related to abnormal BBB permeability in several pathological conditions, such as traumatic brain injury, vascular cognitive impairments, brain tumors, and various neurodegenerative diseases [24, 25]. The method can also operate synergistically with other imaging modalities such as optoacoustics, micro-CT or -MRI by filling imaging gaps in terms of capillary level resolution or imaging speed.

In conclusion, we proposed a widefield fluorescence localization microscopy method capable of rendering the entire murine cerebral vasculature at capillary level resolution together with accurate information on blood circulation velocity and direction. WFLM is easy-to-implement, cost-effective, quantitative and robust. The high spatial resolution and quantitative functional information are poised to greatly aid the assessment of brain function in health and disease.

Funding. European Union's Horizon 2020 Marie Skłodowska-Curie Grant No. 746430 and the European Research Council Consolidator Grant ERC-2015-CoG-682379.

Acknowledgement. The authors would like to thank M. Reiss for assistance with animal experimentation.

Disclosures. The authors declare no conflicts of interest.

References

1. I. Vanzetta, J Physiol Paris **100**, 201 (2006).
2. J. Liu, Y. Wang, Y. Akamatsu, C. C. Lee, R. A. Stetler, M. T. Lawton, and G. Yang, Prog Neurobiol **115**, 138(2014).
3. M. D. Sweeney, K. Kisler, A. Montagne, A. W. Toga, and B. V. Zlokovic, Nat Neurosci **21**, 1318 (2018).
4. S. Watkins, S. Robel, I. F. Kimbrough, S. M. Robert, G. Ellis-Davies, and H. Sontheimer, Nat Commun **5**, 4196 (2014).
5. T. Miyawaki, S. Morikawa, E. A. Susaki, A. Nakashima, H. Takeuchi, S. Yamaguchi, H. R. Ueda, and Y. Ikegaya, Nat Commun **11**, 1104 (2020).
6. A. T. Wassie, Y. Zhao, and E. S. Boyden, Nat Methods **16**, 33 (2019).
7. S. Fantini, A. Sassaroli, K. T. Tgavalekos, and J. Kornbluth, Neurophotonics **3**, 31411 (2016).
8. B. Laviña, Int J Mol Sci **18**, 70 (2016).
9. H. Estrada, J. Rebling, W. Sievert, D. Hladik, U. Hofmann, S. Gottschalk, S. Tapio, G. Multhoff, and D. Razansky, Bone, 115251 (2020).
10. Z. Chen, X. L. Dean-Ben, S. Gottschalk, and D. Razansky, Opt Lett **42**, 4577 (2017).
11. R. K. Wang, and S. Hurst, OPT EXPRESS **15**, 11402 (2007).
12. U. Baran, and R. K. Wang, NEUROPHOTONICS 3, 10902 (2016).
13. J. D. Briers, and S. Webster, J Biomed Opt **1**, 174 (1996).
14. V. Kalchenko, D. Israeli, Y. Kuznetsov, and A. Harmelin, Sci Rep-Uk **4**, 5839 (2014).
15. J. R. G., and D. B. J., in IEE Colloquium on Biomedical Applications of Photonics (Digest No. 1997/124), p. 11.
16. A. Nadort, K. Kalkman, T. G. van Leeuwen, and D. J. Faber, Sci Rep-Uk **6**, 25258 (2016).
17. J. Tinevez, Simpletracker [software] (2020), https://www.github.com/tinevez/simpletracker.
18. A. Serov, and T. Lasser, Opt Express **13**, 6416 (2005).
19. Z. Chen, B. Mc Larney, J. Rebling, X. L. Deán-Ben, Q. Zhou, S. Gottschalk, and D. Razansky, Laser Photonics Rev, 1900070 (2019).
20. C. Vinegoni, S. Lee, A. D. Aguirre, and R. Weissleder, FRONT PHYSIOL **6**, 147 (2015).
21. S. Lee, C. Vinegoni, P. F. Feruglio, L. Fexon, R. Gorbatov, M. Pivoravov, A. Sbarbati, M. Nahrendorf, and R. Weissleder, NAT COMMUN **3**, 1054 (2012).
22. B. Huang, W. Wang, M. Bates, and X. Zhuang, Science **319**, 810 (2008).
23. G. Grover, K. DeLuca, S. Quirin, J. DeLuca, and R. Piestun, Opt Express **20**, 26681 (2012).
24. N. R. Saunders, K. M. Dziegielewska, K. Møllgård, and M. D. Habgood, Front Neurosci-Switz **9**, 385 (2015).
25. R. Natarajan, N. Northrop, and B. Yamamoto, Current protocols in neuroscience **79**, 9 (2017).